

Investigation of chemical bath deposition of ZnO thin films using six different complexing agents

Hani Khallaf¹, Guangyu Chai¹, Oleg Lupan^{1,2}, Helge Heinrich^{1,3}, Sanghoon Park¹, Alfons Schulte¹ and Lee Chow^{1,3,4}

¹ Department of Physics, University of Central Florida, Orlando, FL 32816, USA

² Department of Microelectronics and Semiconductor Devices, Technical University of Moldova, 168 Stefan cel Mare Boulevard, MD-2004 Chisinau, Republic of Moldova

³ Advanced Materials Processing and Analysis Center, Department of Mechanical, Materials and Aerospace Engineering, University of Central Florida, Orlando, FL 32816, USA

E-mail: chow@mail.ucf.edu

Received 11 March 2009, in final form 27 April 2009

Published 17 June 2009

Online at stacks.iop.org/JPhysD/42/135304

Abstract

Chemical bath deposition of ZnO thin films using six different complexing agents, namely ammonia, hydrazine, ethanolamine, methylamine, triethanolamine and dimethylamine, is investigated. As-grown films were mainly ZnO₂ with a band gap around 4.3 eV. Films annealed at 400 °C were identified as ZnO with a band gap around 3.3 eV. X-ray diffraction and micro-Raman spectroscopy revealed that as-grown films consist mainly of cubic zinc peroxide that was transformed into hexagonal ZnO after annealing. Rutherford backscattering spectroscopy (RBS) detected excess oxygen content in ZnO films after annealing. Fourier transform infrared spectroscopy of as-grown films showed a broad absorption band around 3300 cm⁻¹ suggesting that the as-grown films may consist of a mixture of zinc peroxide and zinc hydroxide. X-ray photoelectron spectroscopy multiplex spectra of the O 1s peak were found to be consistent with film stoichiometry revealed by RBS. High-resolution transmission electron micrographs showed small variations of the order of 10 nm in film thickness which corresponds to the average grain size. A carrier density as high as 2.24 × 10¹⁹ cm⁻³ and a resistivity as low as 6.48 × 10⁻¹ Ω cm were obtained for films annealed at 500 °C in argon ambient.

(Some figures in this article are in colour only in the electronic version)

1. Introduction

Chemical bath deposition (CBD) is known to be a simple, low temperature and inexpensive large-area deposition technique. It has been widely used in the deposition of groups II–VI semiconductors thin films, such as CdS [1, 2], CdSe [3, 4], CdO [5, 6], ZnS [7, 8], ZnSe [9, 10] and ZnO [11–20]. Several complexing agents have been employed in CBD of ZnO thin films. Saeed and O'Brien [11] reported deposition of good-quality ZnO thin films using ethylenediamine (EDA) at pH values of 10.5–11. Films grown at pH 10 or less

were powdery, spotted and non-uniform and could be easily removed by abrasion with a tissue. The starting bath pH of 9.0–9.1 was raised to 10.0–11.0 by the addition of NaOH. The band energy of the ZnO films grown was found to be 3.15 eV [11, 12]. Ortega-López and Morales-Acevedo [13] reported CBD of ZnO using NH₄OH and H₂O₂ (30%) at pH values of 10.5–11.2. They found that using H₂O₂ is essential for obtaining polycrystalline ZnO. All films grown in the absence of hydrogen peroxide were amorphous for any deposition temperature and they continued to be amorphous after annealing. The grown films before and after annealing showed a band gap of 4.2 eV and 3.3 eV, respectively. In another work [14], they have added NH₄Cl as a buffer and

⁴ Author to whom any correspondence should be addressed.

reported a slower deposition rate. The band gap values of as-grown and annealed films were 4.2 eV and 3.25 eV, respectively.

Ennaoui *et al* [15], however, reported CBD as well as successive ionic layer adsorption and reaction (SILAR) of ZnO using NH_4OH only. Mikami *et al* [16] investigated both EDA and NH_4OH as complexing agents for CBD of ZnO and concluded that the growth of ZnO is unstable for the perturbation of EDA concentration. They reported that films grown with EDA showed quite poor adhesion and poor uniformity, while films grown with ammonia showed good adhesion and uniformity. They considered $\text{Zn}(\text{OH})_2$ as the ZnO precursor in their work, and showed numerically that in the case of ammonia, the concentration of $\text{Zn}(\text{OH})_2$ is almost constant in a wide range of ammonia concentrations. However, in the case of EDA, the concentration of $\text{Zn}(\text{OH})_2$ is strongly dependent on the EDA concentration in solution. The ZnO film was reported to have a band gap of 3.4 eV and a resistivity of $10^9 \Omega \text{ cm}$. Drici *et al* [18] grew adherent but non-specular ZnO films using EDA at a fixed pH value of 11.0, with the help of NaOH. They reported a resistivity of the order of $10^4 \Omega \text{ cm}$, measured with a two point electrodes longitudinal structure with an electrode gap of 2 mm.

Ouerfelli *et al* [19] reported a five orders of magnitude drop in resistivity of CBD-ZnO films annealed under vacuum compared with those annealed in air. All ZnO films were grown using EDA at a fixed pH value of 11.0, with the help of NaOH. Peiró *et al* [20] reported growing nanostructured ZnO thin films using zinc nitrate/zinc acetate as Zn-precursor and urea/hexamethylenetetramine as complexing agents. They have shown that microwave activated CBD-ZnO films are crystalline and no additional heat treatment/annealing is necessary. In this work, CBD of ZnO thin films using six different complexing agents, namely ammonia, hydrazine (N_2H_4), ethanolamine (EA) $\text{C}_2\text{H}_7\text{NO}$, methylamine (MA) CH_3NH_2 , triethanolamine (TEA) $\text{C}_6\text{H}_{15}\text{NO}_3$ and dimethylamine (DMA) $\text{C}_2\text{H}_7\text{N}$, is investigated. ZnSO_4 is used as zinc source and H_2O_2 is used as an oxidation agent. Transmittance, reflectance measurements and band gap calculations are carried out for as-grown films as well as annealed films. Resistivity, carrier density and Hall mobility of annealed films are acquired using Hall effect measurements. Crystal structure as well as crystal quality are determined using x-ray diffraction (XRD), transmission electron microscopy (TEM), Fourier transform infrared spectroscopy (FTIR) and micro-Raman spectroscopy. Film morphology, composition and binding energy are studied using scanning electron microscopy (SEM), Rutherford backscattering spectroscopy (RBS) and x-ray photoelectron spectroscopy (XPS), respectively.

2. Experimental details

ZnO films were prepared using aqueous solutions of ZnSO_4 (0.014 M), H_2O_2 (34%) and NH_4OH (29.4%). Each bath contained 100–120 ml of de-ionized water (resistivity $\sim 18.2 \text{ M}\Omega \text{ cm}$) that was kept under stirring at 85°C . In addition to ammonia, five more complexing agents were used: N_2H_4 ,

EA, MA, TEA and DMA. To ensure stable $\text{Zn}[\text{NH}_3]_4^{+2}$ complex in the main solution, ammonia was added whenever one of these five complexing agents was being used. It was noticed that adding ammonia is necessary to dissolve the $\text{Zn}(\text{OH})_2$ formed upon mixing the Zn-source and any of the five aforementioned complexing agents. ZnSO_4 and the desired complexing agent were mixed at room temperature before being added to the main solution. Appropriate amounts of hydrogen peroxide were then added to the main solution. Films were grown on a $38 \text{ mm} \times 38 \text{ mm} \times 1 \text{ mm}$ glass substrates (Schott Borofloat glass). With the help of a Teflon holder, the glass substrate was kept vertically in the solution. All substrates were held in the bath prior to the addition of any of the reagents. To ensure deposition of high quality, adhesive and specularly reflecting films, the substrate was removed from the solution when the solution became turbid and the homogeneous reaction started to take place. The cleaning steps of the substrate are reported elsewhere [21].

Specular transmittance measurements were carried out at room temperature with unpolarized light at normal incidence in the wavelength range from 250 to 1100 nm using a Cary 500 (Varian) double beam UV/VIS spectrophotometer. Specular reflectance measurements were performed at an angle of incidence of 7° in the same wavelength range. The optical absorption coefficient α was calculated for each film using the equation [22]:

$$T = (1 - R)^2 \exp(-\alpha t), \quad (1)$$

where T is the transmittance, R is the reflectance and t is the film thickness.

The absorption coefficient α is related to the incident photon energy $h\nu$ as

$$\alpha = \frac{K (h\nu - E_g)^{n/2}}{h\nu}, \quad (2)$$

where K is a constant, E_g is the optical band gap and n is equal to 1 for direct band gap material such as ZnO. The band gap was determined for each film by plotting $(\alpha h\nu)^2$ versus $h\nu$ and then extrapolating the straight line portion to the energy axis. Resistivity, Hall mobility and carrier density were evaluated by Hall effect measurements at room temperature in a Van der Pauw four-point probe configuration, using indium contacts, in an automated Hall effect system (Ecopia HMS-3000, Bridge Technology, Chandler Heights AZ, USA) with a 0.55 T magnetic induction. XRD was carried out using Rigaku D XRD unit (with 40 kV, 30 mA $\text{CuK}\alpha$ radiation, $\lambda = 0.15406 \text{ nm}$). The sample was mounted at 2.5° and scanned from 30° to 70° in steps of 0.02° with a scan rate of $1.2^\circ \text{ min}^{-1}$. TEM was performed using a Tecnai F30 TEM system operating at an acceleration voltage of 300 kV. Cross sections of ZnO films were prepared with FEI 200 focused ion beam system. Micro-Raman scattering was performed at room temperature with a Horiba Jobin Yvon LabRam IR system at a spatial resolution of $2 \mu\text{m}$ in a backscattering configuration. A 632.8 nm line of a helium neon laser was used for off-resonance excitation with less than 4 mW power at the sample. The spectral resolution was 2 cm^{-1} , and

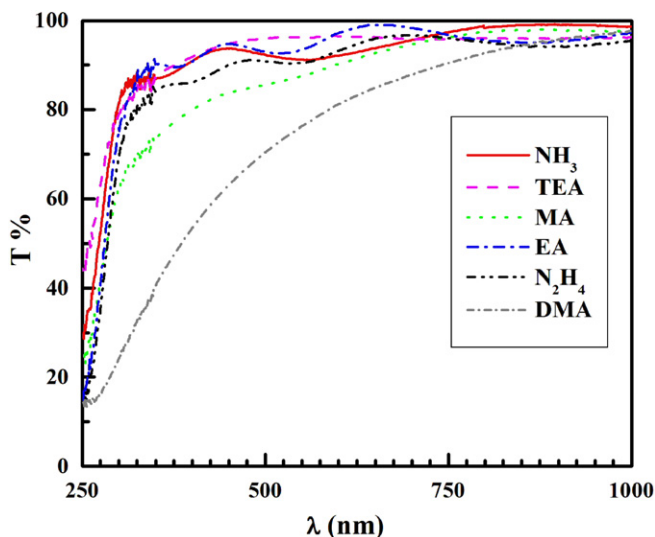


Figure 1. Specular transmittance of as-grown ZnO films deposited using six different complexing agents.

the instrument was calibrated to the same accuracy using a naphthalene standard. The FTIR micro-analysis was carried out at room temperature using contact ATR optimized objective that covers a range of wavenumbers from 650 to 4000 cm^{-1} . SEM micrographs were obtained using a JEOL 6400F SEM at an acceleration voltage of 10 kV. XPS was performed on a Physical Electronics PHI 5400 ESCA using unmonochromated Mg $K\alpha$ radiation at 1253.6 eV. Each of the XPS spectra was acquired from 30 repeated sweeps. XPS spectra were corrected from charging effects by referencing the adventitious C 1s peak to 284.6 eV. RBS measurements were carried out using 2.25 MeV α -particles from General IONIX Tandetron, with a surface barrier detector with energy resolution ≤ 15 keV (full width at half maximum—FWHM), positioned at a scattering angle of 165°.

3. Results and discussion

Figure 1 shows the optical transmittance of as-grown films for all six complexing agents. As shown, five of these films exhibit a sharp absorption edge around 280–290 nm and a high transmittance that exceeds 80% in the visible region. The films grown using DMA, however, were of poor quality. It was noticed that when using DMA, the homogeneous reaction quickly dominated over the heterogeneous reaction and all films grown were whitish, non-uniform and extremely thin (less than 500 Å). Such poor quality is responsible for the absence of a clear absorption edge and the low transmittance observed in the case of DMA-based films. As a result, these films were discarded from any further characterizations. Films grown using other five ligands were adhesive, transparent, uniform and specularly reflecting with a thickness in the range 0.2–0.7 μm . To ensure full conversion to ZnO, as-grown films were annealed at 400 °C in air for 1 h. It was noticed that the quality of EA-based films deteriorated upon annealing and these films lost their integrity and became flakes-like. Annealing at lower temperatures, such as 200 and 300 °C in air

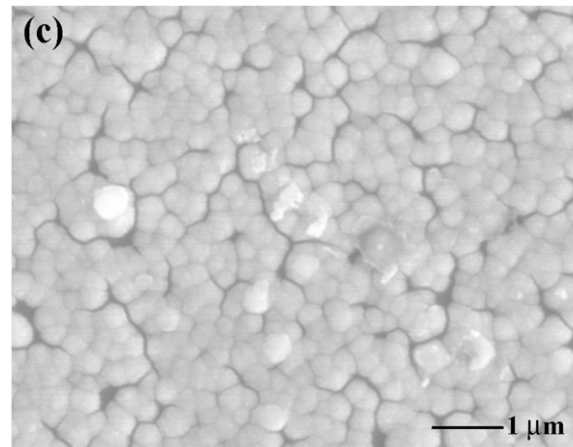
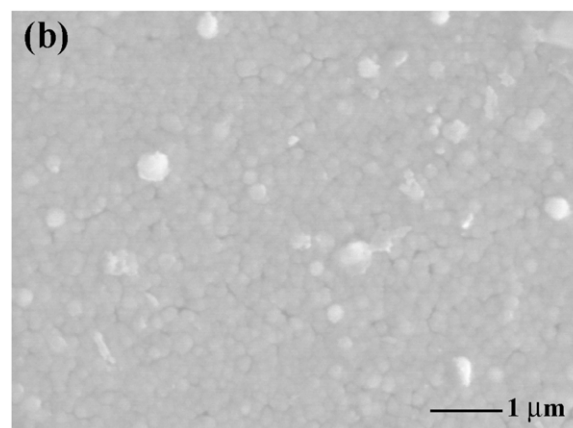
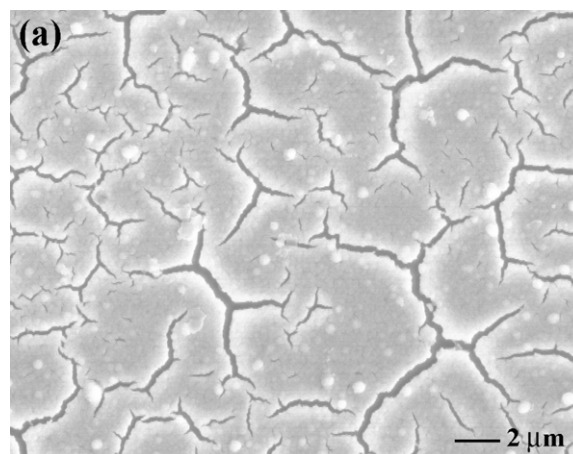


Figure 2. SEM micrographs of (a) as-grown EA-based film, (b) as-grown MA-based film and (c) annealed MA-based film.

as well as in ambient argon had the same effect on all EA-based films. Apparently, there is too much stress in EA-based films that resulted in a high density of cracks as shown in figure 2(a). Post-heat treatments induced further stress in the films which in turn caused the films to lose their integrity and thus become flakes-like, as observed under optical microscope. Films grown using ammonia, N_2H_4 , MA and TEA maintained the same quality after annealing. SEM micrographs of as-grown as well as annealed MA-based film are shown in figures 2(b) and (c). As shown, other than an increase in grain size after

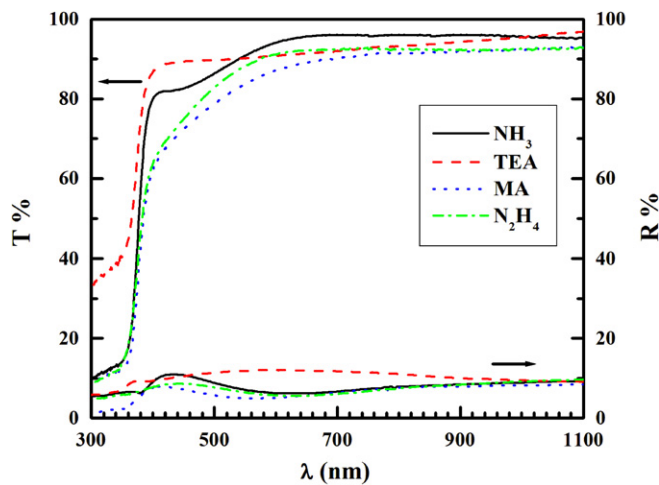


Figure 3. Specular transmittance and reflectance of NH₃, N₂H₄, MA and TEA-based annealed films.

Table 1. A summary of the optical band gap of as-grown and annealed ZnO films.

Complexing agent	Optical band gap (eV)	
	As-grown film	Annealed film
NH ₃	4.35	3.27
N ₂ H ₄	4.29	3.27
TEA	4.38	3.30
MA	4.27	3.25
EA	4.30	—
DMA	3.75	—

annealing, film quality remains almost the same. Further characterizations are therefore limited to films grown using ammonia, N₂H₄, MA and TEA only.

Figure 3 shows the optical transmittance and reflectance of ZnO films annealed at 400 °C in air. All films maintain their quality after annealing and show a better transmission that exceeds 90% right before the absorption edge. The absorption edge of annealed films is sharper than that of as-grown films. This indicates an enhancement in film crystallinity after annealing. The absorption edge observed is around 375–380 nm. Table 1 summarizes the band gap of as-grown films as well as annealed films. Figure 4 shows the typical red shift observed after annealing for ZnO films grown using N₂H₄. The band gap values calculated for as-grown films agree with what has been reported earlier for Zn(OH)₂/ZnO₂ [13, 14], while the band gap values calculated for annealed films agree well with the 3.3 eV band gap of single crystalline ZnO [23].

According to the XRD pattern shown in figure 5(a), TEA-based as-grown films are polycrystalline and consist mainly of cubic zinc peroxide with a preferential orientation along the [200] direction. Other phases of hexagonal ZnO as well as traces of elemental zinc have been detected. No diffraction peaks of Zn(OH)₂ have been observed. Similar XRD patterns of ZnO₂ have been reported by Ortega-López *et al* [14], Han *et al* [24] and Hsu C and Wu [25]. We believe that using hydrogen peroxide as an oxidation agent resulted in the formation of ZnO₂ instead of Zn(OH)₂. This agrees with results reported earlier in the literature [14, 24–28].

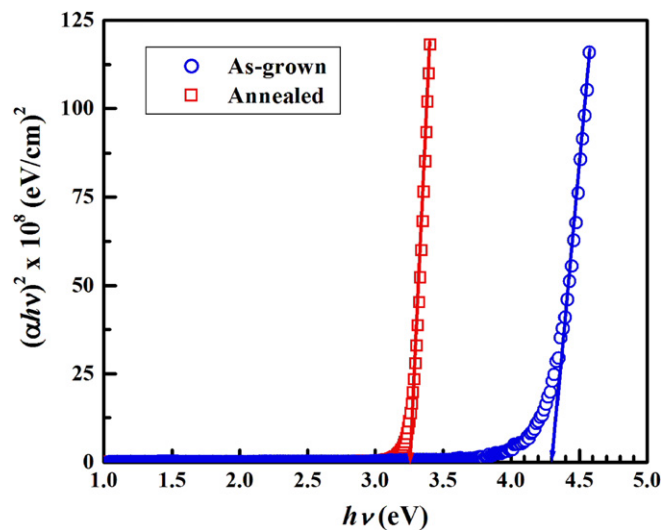


Figure 4. Optical band gap calculations of as-grown and annealed N₂H₄-based film.

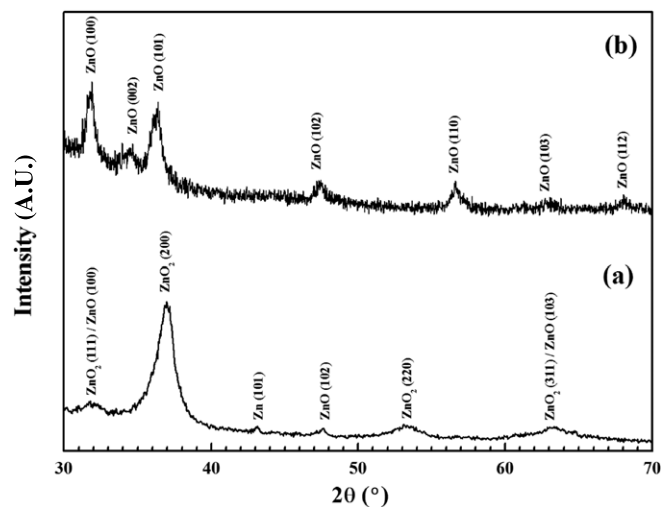


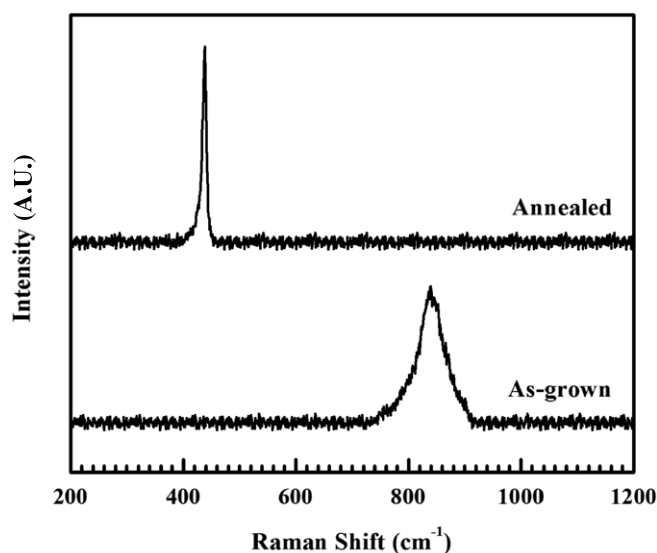
Figure 5. XRD pattern of (a) as-grown TEA-based film and (b) annealed TEA-based film.

Figure 5(b) shows the XRD pattern of the same film after annealing at 400 °C in air for 1 h. As shown, only diffraction peaks of hexagonal ZnO have been detected. Annealed films are polycrystalline with preferred orientation along the [1 0 1] direction with no cubic phases of ZnO₂ been detected. A summary of XRD data for standard cubic ZnO₂, hexagonal ZnO and elemental zinc as well as XRD data of as-grown and annealed films is shown in table 2.

Micro-Raman spectra of MA-based as-grown and annealed films are shown in figure 6. The peak observed at 840 cm⁻¹ for as-grown film is attributed to ZnO₂ and has been reported earlier by Uekawa *et al* [26] and Sun *et al* [27]. Uekawa *et al* [26] assigned this peak to the stretching band of the O–O bond of the peroxo ion (O₂²⁻). After annealing, the peak at 840 cm⁻¹ disappeared and only one peak at 437.2 cm⁻¹ was observed, which is the characteristic peak of the non-polar Raman active E₂-high mode of ZnO [32, 33]. A Lorentzian fit of the peaks at 840 cm⁻¹ and 437.2 cm⁻¹ showed a FWHM of 58.7 cm⁻¹ and 7.8 cm⁻¹, respectively. The observed reduction

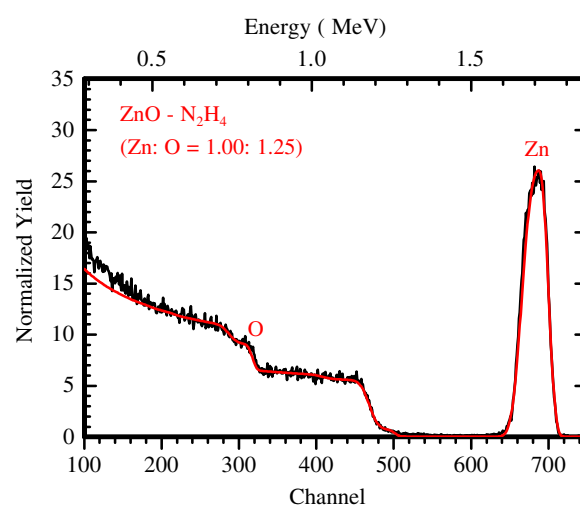
Table 2. A summary of XRD data for standard cubic ZnO₂, hexagonal ZnO, elemental Zn and as-grown and annealed TEA-based film.

Sample	2 θ (°)	d (nm)	I/I ₀ (%)	(h k l)	Sample	2 θ (°)	d (nm)	I/I ₀ (%)
ZnO ₂ (Cubic) [29]	31.794	0.281 23	65.5	(1 1 1)	As-grown film	31.786	0.281 29	10.6
	36.876	0.243 55	100.0	(2 0 0)		36.950	0.243 08	100.0
Zn (Hexagonal) [30]	43.220	0.209 15	100.0	(1 0 1)		43.147	0.209 50	7.1
ZnO (Hexagonal) [31]	47.535	0.191 13	21.1	(1 0 2)		47.547	0.191 08	7.9
ZnO ₂ (Cubic) [29]	53.139	0.172 22	44.1	(2 2 0)		53.142	0.172 21	7.5
	63.268	0.146 87	39.1	(3 1 1)		63.350	0.146 69	6.7
ZnO (Hexagonal) [31]	31.766	0.281 47	56.5	(1 0 0)	Annealed film	31.761	0.281 51	89.2
	34.419	0.260 36	41.5	(0 0 2)		34.437	0.260 22	21.9
	36.250	0.247 61	100.0	(1 0 1)		36.379	0.246 76	100.0
	47.535	0.191 13	21.1	(1 0 2)		47.459	0.191 41	26.1
	56.590	0.162 51	30.5	(1 1 0)		56.638	0.162 38	39.3
	62.851	0.147 74	26.8	(1 0 3)		62.739	0.147 98	15.0
	67.941	0.137 86	21.7	(1 1 2)		68.041	0.137 68	21.1

**Figure 6.** Raman spectra of as-grown and annealed MA-based film.

in FWHM after annealing indicates an enhancement in film crystallinity as is suggested by the SEM and the transmittance measurements reported earlier (figures 2 and 3). It should be noted that the baseline noise in the micro-Raman spectra is estimated to be about 6% of the peak height. As a result, it is not surprising that no vibration modes of ZnO were observed for the as-grown films. As table 2 shows, the relative intensity of the (1 0 2) peak of ZnO to that of the (2 0 0) peak of ZnO₂ in the as-grown film is about 7.9%. Such a low percentage of the hexagonal phase of ZnO in the as-grown film compared with that of the cubic phase of ZnO₂ may be the reason for not detecting any vibration modes of ZnO in the as-grown films.

Figure 7 shows the RBS spectra of N₂H₄-based film annealed at 400 °C in air for 1 h. Simulation using Rutherford Universal Manipulation Program (RUMP) [34] was implemented to obtain the best possible match to the raw RBS spectra. As shown, the Zn : O ratio obtained for the annealed film was (1.00 : 1.25). Since ZnO films are inherently n-type in nature, which is due to either oxygen deficiency in the film or zinc ions existing in interstitial positions, a ratio of Zn : O of less than unity was unexpected. RBS carried out on films grown using MA as well as NH₃ that are annealed under the

**Figure 7.** RBS spectrum and RUMP simulation of annealed N₂H₄-based film.

same conditions (not shown in this work), also detected more oxygen content than zinc in both films. Because of their high resistivity, we were not able to perform Hall measurements on films annealed at 400 °C.

Although both XRD and micro-Raman spectroscopy are suggesting that as-grown films are mainly zinc peroxide, FTIR absorption spectroscopy of MA-based as-grown film, as shown in figure 8, detects a broadband around 3300 cm⁻¹ which is assigned to the O–H stretching mode of the hydroxyl group. This suggests that as-grown films may consist of a mixture of zinc peroxide and zinc hydroxide. Peaks detected between 2840 and 2930 cm⁻¹ are due to the C–H stretching vibration mode, which corresponds to the CH₃ group of methylamine. Similar observation has been reported earlier by Ortega-López and Morales-Acevedo [13], where they detected a broad absorption band with a peak at 3354 cm⁻¹ related to the longitudinal stretching mode (3380 cm⁻¹) of the OH group. Xiong *et al* [35] observed the same stretching mode at 3500 cm⁻¹ for ZnO nanoparticles grown via plasma synthesis.

Figure 9(a) shows the XPS multiplex spectra of the O 1s peak for as-grown as well as annealed TEA-based film. The binding energy of the O 1s peak of as-grown film is located at 532.0 eV. According to Dupin *et al* [36], binding energies of

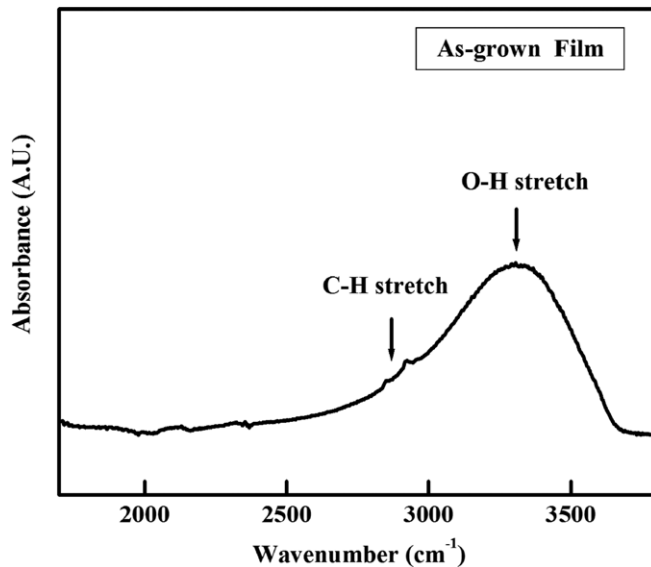


Figure 8. FTIR absorbance spectrum of as-grown MA-based film.

the O 1s peak in the range 527.7–530.6 eV are characteristics of O^{2-} oxides, and binding energies in the range 530.6–531.1 eV are characteristic of oxygen species integrated in the material as OH^- or O_2^{2-} , while binding energies in the range 531.1–532.0 eV are due to low coordinated oxygen ions that could be described as ' O^- ' species. However, it should be noted that binding energies as high as 532.8 and 533.6 eV have been reported earlier for peroxides and hydro-peroxides at polymer surfaces [37]. Therefore, considering the findings of the XRD and micro-Raman (figures 5 and 6), we believe that the binding energy observed in this work at 532.0 eV is attributed to zinc peroxide. A shift of about 2.0 eV was observed for the O 1s peak of the annealed film.

Figure 9(b) shows the XPS multiplex of the Zn $2p_{3/2}$ peak. The binding energy of the Zn $2p_{3/2}$ of the as-grown film was observed at 1022.2 eV, while the binding energy associated with the Zn $2p_{3/2}$ peak of the annealed film is 1021.8 eV, which indicates a small shift of 0.4 eV after annealing. Both values are within the range of binding energy characteristics of ZnO [38]. Since the O 1s peak of the annealed film is asymmetric, a deconvolution of this peak was carried out, as shown in figure 9(c). As shown, deconvolution of the O 1s peak of the annealed ZnO film renders two doublets with the main doublet located at 530.0 eV, and the smaller one located at 531.8 eV. The contribution observed at 530.0 eV is a characteristic of O^{2-} oxides [36, 38], while the contribution at 531.8 eV is due to either peroxide or ' O^- ' species. This explains the excess oxygen content in the ZnO film after annealing at 400 °C that was detected by RBS (figure 7). Since it is widely believed that zinc peroxide completely decomposes into zinc oxide at annealing temperatures higher than 200 °C [24–26], we believe that the contribution at 531.8 eV is mainly due to low coordinated ' O^- ' species, as suggested by Dupin *et al* [36]. The presence of such low coordinated ' O^- ' species in the film could be attributed to the chemisorption of oxygen at the grain boundaries during the CBD process [39, 40].

High-resolution transmission electron microscopy (HRTEM) of NH_3 -based ZnO film that was annealed at 400 °C

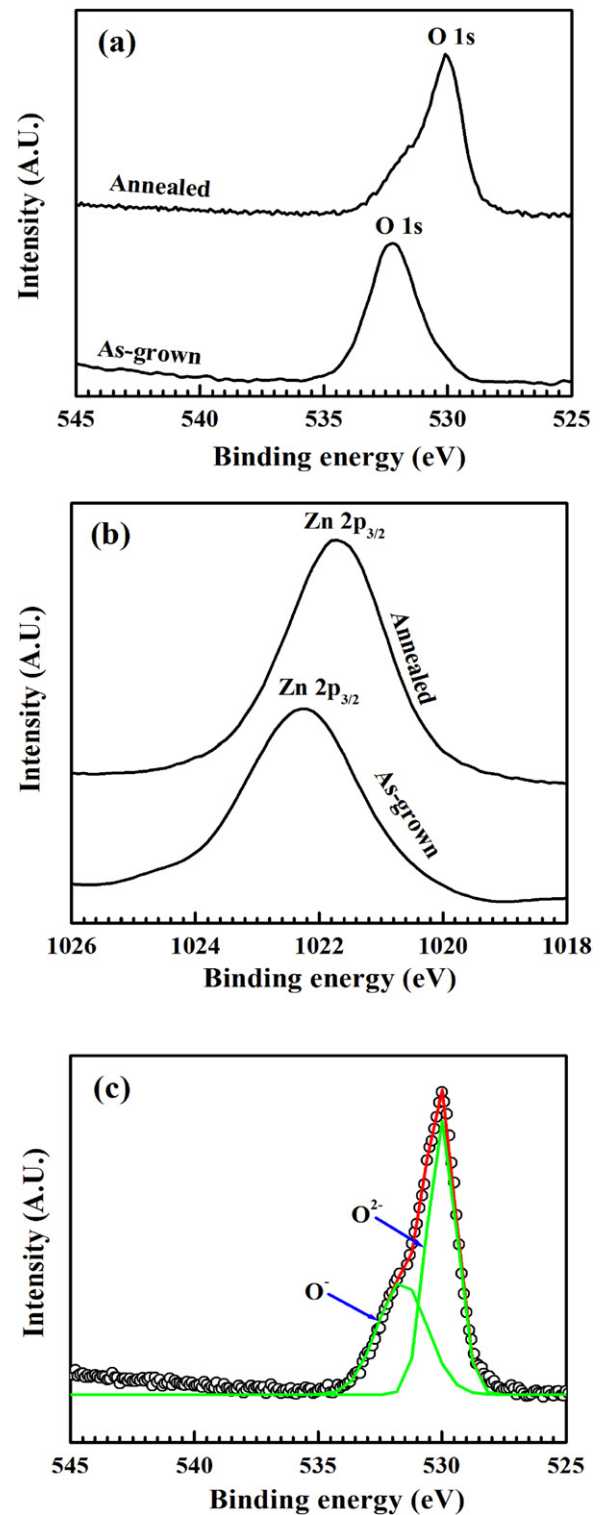


Figure 9. (a) XPS multiplex spectra of O 1s of as-grown and annealed TEA-based film. (b) XPS multiplex spectra of Zn $2p_{3/2}$ of as-grown and annealed TEA-based film. (c) Deconvolution of the O 1s peak of annealed TEA-based film.

in air is shown in figure 10(a). As shown, the ZnO layer is about 0.2 μm and the average grain size is about 10 nm. Only small variations in film thickness are observed, which are in the range of the 10 nm average grain diameter. Occasional cracks due to annealing are found at the surface of the film,

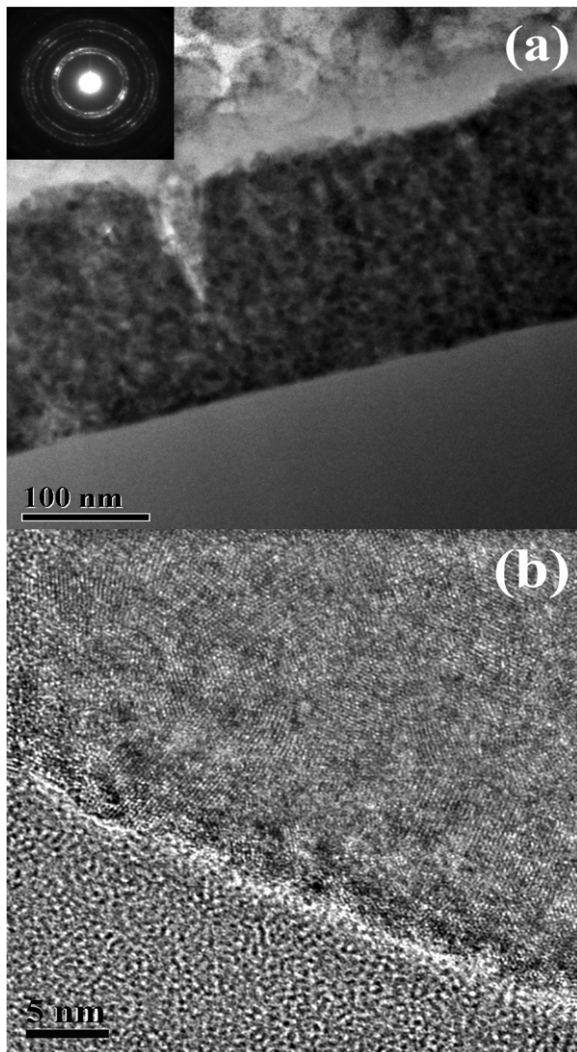


Figure 10. (a) HRTEM and TEM diffraction pattern (inset) of annealed NH₃-based ZnO film. (b) Fourier-filtered HRTEM of annealed NH₃-based ZnO film (low boundary is glass substrate).

which typically extend about half way into the ZnO layer. The electron diffraction pattern observed (inset of figure 10(a)) confirms that the ZnO film is polycrystalline with a hexagonal crystal lattice. The Fourier-filtered HRTEM image in figure 10(b) shows the crystal structure of the individual ZnO grains and their size.

As mentioned earlier, films annealed at 400 °C were highly resistive and, as a result, performing Hall measurements on such films was not possible. Therefore, the films used for Hall measurements were further annealed at 500 °C in ambient argon for 1 h. The carrier density, resistivity and Hall mobility of the films grown using ammonia, N₂H₄, MA and TEA are shown in table 3. As shown, all films show high carrier density and low resistivity for CBD undoped ZnO films. A carrier density as high as $2.24 \times 10^{19} \text{ cm}^{-3}$ and a resistivity as low as $6.48 \times 10^{-1} \Omega \text{ cm}$ were obtained. This may be a good indication that future *in situ* doping of CBD-ZnO films using group III elements, such as aluminium, boron, indium or gallium may reduce the resistivity further to achieve transparent conducting CBD-ZnO thin films.

Table 3. Hall effect measurements of NH₃, N₂H₄, MA and TEA-based annealed ZnO films.

Sample	Carrier density (cm ⁻³)	Mobility (cm ² V ⁻¹ S ⁻¹)	Resistivity (Ω cm)
NH ₃ -based	1.52×10^{19}	1.01×10^{-1}	4.04×10^0
MA-based	2.03×10^{18}	1.37×10^{-1}	2.23×10^1
TEA-based	1.02×10^{19}	9.44×10^{-1}	6.48×10^{-1}
N ₂ H ₄ -based	2.24×10^{19}	1.1×10^{-2}	2.51×10^1

4. Conclusion

CBD of ZnO thin films using six different complexing agents is investigated. Four of these six ligands proved to be successful where high quality, adherent, uniform, transparent and specularly reflecting ZnO films were obtained. As-grown films were mainly ZnO₂ with a band gap around 4.3 eV. Films annealed at 400 °C were ZnO with a band gap around 3.3 eV. XRD and micro-Raman revealed that the as-grown film consists mainly of cubic ZnO₂ that was transformed into hexagonal ZnO after annealing. FTIR of the as-grown film, however, showed a broad absorption band around 3300 cm⁻¹, which is assigned to the O–H stretching mode of the hydroxyl group suggesting that the as-grown film may consist of a mixture of ZnO₂ and Zn(OH)₂. RBS detected excess oxygen content in ZnO films after annealing. XPS spectra were found to be consistent with the RBS observations of the annealed films. HRTEM showed small variations in film thickness in the range of the 10 nm average grain diameter. Occasional cracks, due to annealing, are found at the surface of the film, which typically extend about halfway into the ZnO layer. The electron diffraction pattern observed confirms only a slight texture of the crystal lattice with respect to the substrate. A carrier density as high as $2.24 \times 10^{19} \text{ cm}^{-3}$ and a resistivity as low as $6.48 \times 10^{-1} \Omega \text{ cm}$ were obtained for the annealed ZnO films. One of the challenges we have faced in this work is the strong alkalinity of our solutions that have prevented us from growing thicker ZnO films using multi-dip deposition; any attempt to dip the original film in a fresh solution to grow another layer of ZnO resulted in immediate etching of the original layer and a subsequent deposition of a non-uniform and a porous new ZnO layer with inferior quality. Therefore, in this work, we were limited to one single deposition with a film thickness that ranged from 0.2 to 0.7 μm. Another challenge was the occasional cracks that appear in ZnO films after annealing, as was revealed by SEM and TEM of annealed MA-based and NH₃-based ZnO films (figures 2 (a) and 10(a), respectively). This, in turn, has a dramatic effect on film Hall mobility, as table 3 indicates. One more challenge we faced is the unexpected excess oxygen content in ZnO films after annealing which resulted in a Zn : O ratio less than unity. As a result, films annealed at 400 °C in air were highly resistive and further annealing at 500 °C in ambient argon was necessary for Hall measurements to be attainable. We believe that more careful post-heat treatments as well as *in situ* doping of such CBD-ZnO films using group III elements, such as aluminium, boron, indium or gallium may reduce the resistivity further where a transparent conducting CBD-ZnO is achievable.

Acknowledgments

The authors are grateful to K Scammon of the Advanced Materials Processing and Analysis Center (AMPAC), University of Central Florida, for his help with the XPS and RBS measurements. The authors are also grateful to Professor Aravinda Kar and his group, especially Mr G Lim, of the College of Optics and Photonics, the University of Central Florida, for their help with the Hall measurements. This work was partially supported by the USDA, Apollo Technologies, Inc., and Florida High Tech Corridor Council.

References

- [1] Khallaf H, Oladeji I and Chow L 2008 *Thin Solid Films* **516** 5967
- [2] Khallaf H, Oladeji I, Chai G and Chow L 2008 *Thin Solid Films* **516** 7306
- [3] Šimurda M, Němec P, Formánek P, Nemeč I, Němcová Y and Malý P 2006 *Thin Solid Films* **511** 71
- [4] Erat S, Metin H and Ari M 2008 *Mater. Chem. Phys.* **111** 114
- [5] Gujar T, Shinde V, Kim W, Jung K, Lokhande C and Joo O 2008 *Appl. Surf. Sci.* **254** 3813
- [6] Ortega M, Santana G and Morales-Acevedo A 2000 *Solid-State Electron.* **44** 1765
- [7] Pudov A, Sites J and Nakada T 2002 *Japan. J. Appl. Phys.* **41** L672
- [8] Cheng J, Fan D, Wang H, Liu B, Zhang Y and Yan H 2003 *Semicond. Sci. Technol.* **18** 676
- [9] Chaparro A, Maffiotte C, Gutiérrez M, Herrero J, Klaer J, Siemer K and Bräunig D 2001 *Thin Solid Films* **387** 104
- [10] Lokhande C, Patil P, Ennaoui A and Tributsch H 1998 *Appl. Surf. Sci.* **123** 294
- [11] Saeed T and O'Brien P 1995 *Thin Solid Films* **271** 35
- [12] O'Brien P, Saeed T and Knowles J 1996 *J. Mater. Chem.* **6** 1135
- [13] Ortega-López M and Morales-Acevedo A 1997 *Proc. 26th Photovoltaic Specialists Conf. (Anaheim, CA, USA)* p 555
- [14] Ortega-López M, Avila-García A, Albor-Aguilera M and Resendiz V 2003 *Mater. Res. Bull.* **38** 1241
- [15] Ennaoui A, Weber M, Scheer R and Lewerenz H 1998 *Sol. Energy Mater. Sol. Cells* **54** 277
- [16] Mikami R, Miyazaki H, Abe T, Yamada A and Konagai M 2003 *3rd World Conf. on Photovoltaic Energy Conversion (Osaka, Japan)* p 519
- [17] Govender K, Boyle D, Kenway P and O'Brien P 2004 *J. Mater. Chem.* **14** 2575
- [18] Drici A, Djeteli G, Tchangbedji G, Derouiche H, Jondo K, Napo K, Bernède J, Ouro-Djobo S and Gbagba M 2004 *Phys. Status Solidi a* **201** 1528
- [19] Ouerfelli J, Regragui M, Morsli M, Djeteli G, Jondo K, Amory C, Tchangbedji G, Napo K and Bernède J 2006 *J. Phys. D: Appl. Phys.* **39** 1954
- [20] Peiró A, Domingo C, Peral J, Domènech X, Vigil E, Hernández-Fenollosa M, Mollar M, Marí B and Ayllón J 2005 *Thin Solid Films* **483** 79
- [21] Khallaf H, Chai G, Lupan O, Chow L, Park S and Schulte A 2008 *J. Phys. D: Appl. Phys.* **41** 185304
- [22] Pankove J 1971 *Optical Processes in Semiconductors* (New York: Dover)
- [23] Sze S 1981 *Physics of Semiconductor Devices* (New York: Wiley)
- [24] Han X, Liu R, Chen W and Xu Z 2008 *Thin Solid Films* **516** 4025
- [25] Hsu C and Wu N 2005 *J. Photochem. Photobiol. A: Chem.* **172** 269
- [26] Uekawa N, Mochizuki N, Kajiwara J, Mori F, Wu Y and Kakegawa K 2003 *Phys. Chem. Chem. Phys.* **5** 929
- [27] Sun M, Hao W, Wang C and Wang T 2007 *Chem. Phys. Lett.* **443** 342
- [28] Lindroos S and Leskela M 2000 *Int. J. Inorg. Mater.* **2** 197
- [29] Joint Committee on Powder Diffraction Standards, Powder Diffraction File No 076-1364
- [30] Joint Committee on Powder Diffraction Standards, Powder Diffraction File No 087-0713
- [31] Joint Committee on Powder Diffraction Standards, Powder Diffraction File No 079-2205
- [32] Damen T, Porto S and Tell B 1966 *Phys. Rev.* **142** 570
- [33] Calleja J and Cardona M 1977 *Phys. Rev. B* **16** 3753
- [34] Doolittle L 1986 *Nucl. Instrum. Methods B* **15** 227
- [35] Xiong G, Pal U, Serrano J, Ucer K and Williams R 2006 *Phys. Status Solidi c* **3** 3577
- [36] Dupin J, Gonbeau D, Vinatier P and Levasseur A 2000 *Phys. Chem. Chem. Phys.* **2** 1319
- [37] Dilks A 1981 *J. Polym. Sci. Polym. Chem. Edn* **19** 1319
- [38] Moulder J, Stickle W, Sobol P and Bomben K 1992 *Handbook of X-ray Photoelectron Spectroscopy* ed J Chastain (Eden Prairie, MN: Perkin-Elmer Corporation)
- [39] Mane R and Lokhande C 2000 *Mater. Chem. Phys.* **65** 1
- [40] Vigil O, Vasco E and Zelaya-Angel O 1996 *Mater. Lett.* **29** 107